Journal of Materials Chemistry C

PAPER

View Article Online
View Journal | View Issue

Cite this: J. Mater. Chem. C, 2019, 7, 8101

Delta-temperatural electronic transportation achieved in metastable perovskite rare-earth nickelate thin films†

Jikun Chen, *[a] Haiyang Hu,[a] Takeaki Yajima,[b] Jiaou Wang,[c] Binghui Ge,[d] Hongliang Dong,[e] Yong Jiang*[a] and Nuofu Chen*[f]

The metal to insulator transition (MIT) in Mott–Hubbard systems is one of the most important discoveries in condensed matter physics, and results in abrupt orbital transitions from insulating to metallic phases by elevating the temperature across a critical point (T_{MIT}). Although the MIT was previously expected to be mainly driven by the orbital Coulomb repulsion energy, the entropy contribution to the orbital free energy, which also determines the relative stability of the metallic and insulating phases, was overlooked. Herein, we demonstrate an additional reversible electronic transition observed in chemically grown thin films of metastable rare-earth nicklate perovskites ($ReNiO_3$) on single crystalline substrates, in addition to their MIT. By elevating the temperature across another critical point ($T_{R\text{-}MIT}$) below T_{MIT}, the resistivity of the $ReNiO_3$/substrate system abruptly increases by 2–3 orders, the transition of which is named reverse temperature-dependence in electrical transportation compared to the metal to insulator transition (denoted herein as the R-MIT) and associated with entropy. $T_{R\text{-}MIT}$ is shown to be enhanced *via* reducing the compositional complexity and size of Re or imparting bi-axial compressive strains, and meanwhile the transition sharpness of delta-temperatural transport is reduced. Combining the afterwards exponentially decreasing resistivity in the insulating phase of $ReNiO_3$ with further temperature elevation, a delta-temperatural transportation character is established. This functionality is potentially useful in locking the working temperature window for electric devices that cater for the demand in the fast developing automatic transmission or artificial intelligence.

Received 2nd May 2019,
Accepted 4th June 2019

DOI: 10.1039/c9tc02327e

rsc.li/materials-c

1. Introduction

The discovery of reversible orbital transitions among multiple-states within electron correlated materials can enrich distinguished material functionalities beyond the conventional and promote new applications.[1–6] The past century witnessed the development of the metal to insulator transition (MIT) discovered in d-band correlated systems,[7–15] which promotes new applications such as thermochromism,[10] thermistors,[11] electronic field effect transistors,[12–14] and neuron-spin logical devices.[15] During the MIT, the orbital configurations within Mott–Hubbard systems experience a sharp transition at a critical temperature (T_{MIT}) that abruptly switches the material phase between a metal and an insulator (semiconductor).[7–9] While previous research focuses on abrupt variations in physical properties across the transition temperature of the MIT (T_{MIT}),[4–16] the intrinsic electrical transportation of the insulating phase far below T_{MIT} was not extensively investigated. Nevertheless, we recently demonstrated that indeed the insulating phase of correlated rare-earth nicklate perovskites ($ReNiO_3$) exhibits a distinguished thermistor transportation behavior with a negative temperature coefficient of resistance (TCR) beyond conventional semiconductors.[11] This indicates the presence of a gradual orbital transition that is sensitive to temperature in the insulating phase of $ReNiO_3$, in addition to their more abrupt Mott transition at T_{MIT}.

Although the MIT was attributed to the reduction in orbital Coulomb energy,[4–15] other perspectives such as the respective variations in orbital configuration entropy ($S_{Orbit.}$) could be also important to the orbital Gibb's free energy ($\Delta G_{Orbit.} = \Delta U_{Coul.} - T\Delta S_{Orbit}$).

[a] Beijing Advanced Innovation Center for Materials Genome Engineering, School of Materials Science and Engineering, University of Science and Technology Beijing, Beijing 100083, China. E-mail: jikunchen@ustb.edu.cn, yjiang@ustb.edu.cn
[b] School of Engineering, The University of Tokyo, 2-11-16 Yayoi, Bunkyo-ku, Tokyo 113-0032, Japan
[c] Beijing Synchrotron Radiation Facility, Institute of High Energy Physics, Chinese Academy of Sciences, Beijing 100049, China
[d] Institute of Physical Science and Information Technology, Anhui University, 230601, Heifei, Anhui, China
[e] Center for High Pressure Science and Technology Advanced Research, Shanghai 201203, China
[f] School of Renewable Energy, North China Electric Power University, Beijing 102206, China. E-mail: nfchen@ncepu.edu.cn

† Electronic supplementary information (ESI) available. See DOI: 10.1039/c9tc02327e

It was also pointed out that the elevation in phonon entropy should be also an important contribution to the MIT of vanadium dioxides when transiting from the low symmetry monoclinic-insulating phase to the high symmetry rutile-metallic phase, as previously pointed out in ref. 16. Recently, several reports on high entropy compounds have highlighted the importance of the large elevation in the configuration entropy to the stability of the material phases, which exceeds the contribution from the enthalpy to the free energy.[17] Beyond reasonable doubt, the synthesizing temperature can be effectively reduced for structural ceramics *via* introducing compositional complexity or enlarging the configurational disorder. Extending an analogical consideration to an electron correlated system with a complex electronic phase diagram, it sheds light on alternative manipulations of the relative stability among multiple electronic phases to seek new intrinsic or extrinsic electronic states and transitions beyond the MIT.

As was previously known, on reducing T from their conventional metallic phase across T_{MIT}, the $ReNiO_3$ experience symmetry breaks in the aspects of both structure (*via* Jahn–Teller distortion) and orbital degeneracy (*via* charge disproportionation).[18–20] Although the reduced symmetry is expected to abruptly decrease S_{Orbit} ($\Delta S_{Orbit.,M\rightarrow I} < 0$), its positive contribution ($-T\Delta S_{Orbit.,M\rightarrow I} > 0$) to $\Delta G_{orbit.}$ is smaller compared to the reduction in $U_{Coul.}$ ($\Delta U_{Coul.M\rightarrow I} < 0$), which dominates the transition from the metallic to the insulating phase. Further cooling is expected to continuously reduce $S_{Orbit.}$ *via* improving the orbital ordering for the disproportionated $t^6_{2g}e^0_g$ (Ni^{2+}) and $t^6_{2g}e^1_g$ (Ni^{4+}) within the insulating phase of $ReNiO_3$, which gradually opens up the electronic band gap.[11] Noticing that this process is more dominated by the variation in the orbital ordering rather than the orbital configuration energy, a more significant temperature induced variation in $S_{Orbit.}$ is expected, compared to the one in $U_{Coul.}$. If there is another critical temperature, at which the magnitude of the positive contribution to $\Delta G_{Orbit.}$ from the entropy aspect ($-T\Delta S_{Orbit.} > 0$) can completely offset the reduction in $U_{Coul,M\rightarrow I}$, it may have the potential to transit the system (*i.e.* integrating together the $ReNiO_3$, their defects and interface) towards a new electronic state.

In this work, we demonstrate the observation of an additional reversible electronic transition in chemically grown metastable $ReNiO_3$ thin films on single crystalline perovskite substrates, apart from their previously known MIT. In such a transition, the resistivity of $ReNiO_3$ abruptly increases by 2–3 orders when elevating T across another critical point ($T_{R\text{-}MIT}$) below T_{MIT}, the transportation of which is in reverse to the MIT and is denoted herein as the R-MIT. This indicates that the temperature range for the stable insulating phase of $ReNiO_3$ should be in between $T_{R\text{-}MIT}$ and T_{MIT}, while the correlated system should transit towards a more conductive state on reducing the temperature below $T_{R\text{-}MIT}$. Noticing that the resistivity of $ReNiO_3$ firstly increases abruptly when elevating T across T_{MIT} and afterwards exponentially decreases *via* its reported NTCR thermistor transportation, it establishes a distinguished character of delta-temperatural transport. By adjusting the rare-earth composition and imparting interfacial strains, the delta-temperatural transport of $ReNiO_3$ can be further regulated, and this new functionality is expected to be used to sense and lock the working temperatures of electronic devices.

2. Experiment

Sample growth

The chemical growth of $ReNiO_3$ includes the following three steps: (1) the chemical precursors of $Re(NO_3)_3$ and $Ni(CH_3COOH)_2$ were mixed at the nominal stoichiometry within ethylene glycol monomethyl ether (EGME) under ultrasound. (2) The as made chemical solutions were spin coated onto single crystalline substrates of $LaAlO_3$, $SrTiO_3$ and $(LaAlO_3)_{0.3}(Sr_2AlTaO_6)_{0.7}$, with the (001) orientation and one side polished, followed by baking at 175 °C to evaporate the EGME. (3) To achieve the crystallization as perovskite $ReNiO_3$, the samples were annealed at 800 °C within an oxygen pressure of 15–20 MPa for 3 hours. Pulsed laser deposition of $SmNiO_3$ was performed by laser ablation of a ceramic target with nominal composition in 20 Pa O_2 pressure within a vacuum chamber. During the deposition, the temperature of the $SrTiO_3$ substrate was kept at 650 °C. After the deposition process, the as obtained sample was annealed within an oxygen pressure of 15 MPa for 3 hours.

Characterization

A commercial CTA-system was used to measure the resistivity of the as-grown thin films in the high temperature range within 300–550 K, while a PPMS system from Quantum Design was used to characterize their resistance in the low temperature range within 5–400 K and under external magnetic fields. The cross-plane and in-plane information of the as-grown films compared to the substrates were probed by using reciprocal space mapping (RSM). The [114] reciprocal space vectors of both the film and substrate are projected on the [110] and [001] reciprocal vectors for the in-plane and cross-plane direction, respectively. To characterize the cross-plane morphology of the as-grown thin films, high-angle annular dark-field (HAADF) and annular bright-field (ABF) scanning transmission electron microscopy (STEM) were performed on a JEM-ARM 200F TEM operated at 200 kV with a cold field emission gun and aberration correctors for both probe-forming and imaging lenses. To characterize the electrical orbital structures, we performed near edge X-ray absorption fine structure (NEXAFS) at the Beijing Synchrotron Radiation Facility, Institute of High Energy Physics, Chinese Academy of Sciences, Beijing 100049, China.

3. Results and discussion

To trigger the as-proposed R-MIT, both the thermodynamic and kinetic aspects need to be taken into account. Thermodynamically, it requires the insulating phase to exhibit more significant variations in $S_{Orbit.}$ compared to the ones in $U_{Coul.}$, when reducing the temperature. In that case, it is possible that the contribution from descending $S_{Orbit.}$ to the $G_{Orbit.}$ of the insulating phase gradually offsets the lower $U_{Coul.}$ of the insulating phase compared to the metallic phase, as illustrated in Fig. 1a. This is expected to

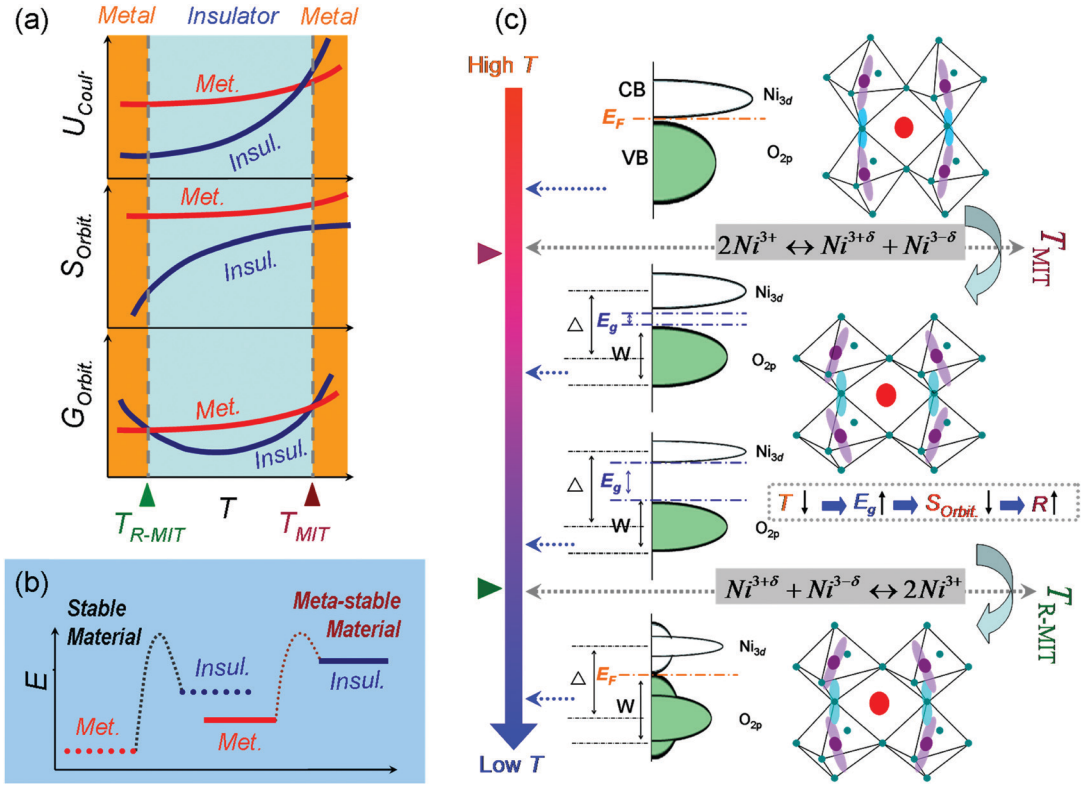

Fig. 1 (a) The temperature dependence of the Coulomb repulsion energy ($U_{Coul.}$), orbital entropy ($S_{Orbit.}$) and free energy ($G_{Orbit.}$) as illustrated for the insulating phase and metallic phase of $ReNiO_3$. By reducing the temperature across T_{MIT}, the $U_{Coul.}$ reduces more significantly for the insulating phase compared to the metallic one, which triggers the conventional metal to insulator transition (MIT). Afterwards, the band gap gradually opens by further reducing the temperature, and the ordering in orbital charge of Ni^{2+} and Ni^{4+} is improved to reduce $S_{Orbit.}$, which elevates the $G_{Orbit.}$ of the insulating phase compared to the metallic one. When reaching $T_{R\text{-}MIT}$, the lower $U_{Coul.}$ of the insulating phase compared to the metallic phase was offset by the reduction in $S_{Orbit.}$ due to the high orbital ordering. Thermodynamically, this is expected to trigger the system to transit towards a new electronic state *via* a reverse metal to insulating transition (R-MIT) with further reduced temperatures. (b) The material metastability is expected to reduce the energy barrier to overcome when triggering the R-MIT. (c) Orbital and structural transformations when the $ReNiO_3$ transforms from a metal to an insulator (MIT) and further to a metal (R-MIT) with a reducing temperature.

be the feature for the insulating phase of $ReNiO_3$, noticing that the NTCR transportation is expected to be more associated with the variation in orbital ordering rather than the orbital potentials. Kinetically, the intrinsic metastability of $ReNiO_3$ elevates the free energies for both its metallic and insulating phases, the effect of which reduces the energy barrier prohibiting the occurrence of the R-MIT at $T_{R\text{-}MIT}$, as illustrated in Fig. 1b. In Fig. 1c, the expected orbital transitions across T_{MIT} and $T_{R\text{-}MIT}$ are illustrated. The metal to insulator transition *via* the MIT when elevating T across T_{MIT} reduces $U_{Coul.}$ and increases $S_{Orbit.}$. This provides the driving force to trigger the system to transform towards another electronic state, *i.e.* with further reduced $U_{Coul.}$ to maintain a negative $\Delta G_{Orbit.}$.

As a typical example, Fig. 2a shows the temperature dependent resistivities (R–T) for quasi-single crystalline $SmNiO_3$ thin films grown on single crystalline perovskite substrates, such as $LaAlO_3$, $SrTiO_3$ and $(La,Sr)(Al,Ta)O_3$, using the chemical approach we described previously.[11] Fig. S1 (ESI†) shows the resistance of the respective samples measured as a function of temperature. We can clearly observe the as-proposed delta temperatural transportation behaviors for all three samples, in which cases the resistivity exponentially increases on reducing T until $T_{R\text{-}MIT}$ (the delta-transition point) and afterwards abruptly reduces. The R–T tendencies measured *via* heating or cooling overlap with each other, indicating that both the R-MIT and its resultant delta-temperature transport are reversible.

It is also worth noticing that a higher T_{Delta} is observed for $SmNiO_3/LaAlO_3$, compared to the ones for $SmNiO_3/SrTiO_3$ and $SmNiO_3/(La,Sr)(Al,Ta)O_3$. According to our previous reports,[11] the lattice mismatch between the film and substrate results in various statuses of interfacial coherency and strain. As can be seen in the cross-section interfacial morphology shown in Fig. 2b, the $SmNiO_3$ film is coherently grown on the $LaAlO_3$ substrate due to a small lattice mismatch ($\sim$0.4%), and is under biaxial compressive interfacial strain. This is in contrast to $SmNiO_3/SrTiO_3$ or $SmNiO_3/(La,Sr)(Al,Ta)O_3$, in which cases the epitaxial coherency is not preservable due to a large lattice mismatch ($\sim -2.4\%$ and -1.6%), and thereby the interfacial strain is relaxed. The X-ray reciprocal space mapping (RSM) results for $SmNiO_3$ grown on the various substrates are further shown in Fig. S2 (ESI†), where the same in-plane lattice vector is observed for $SmNiO_3$ and $LaAlO_3$. In contrast, the in-plane lattice vector for $SmNiO_3$ slightly differs to $(La,Sr)(Al,Ta)O_3$, which indicates a relaxation in the tensile distortion, while the relaxation is more significant for $SmNiO_3/SrTiO_3$. Biaxial

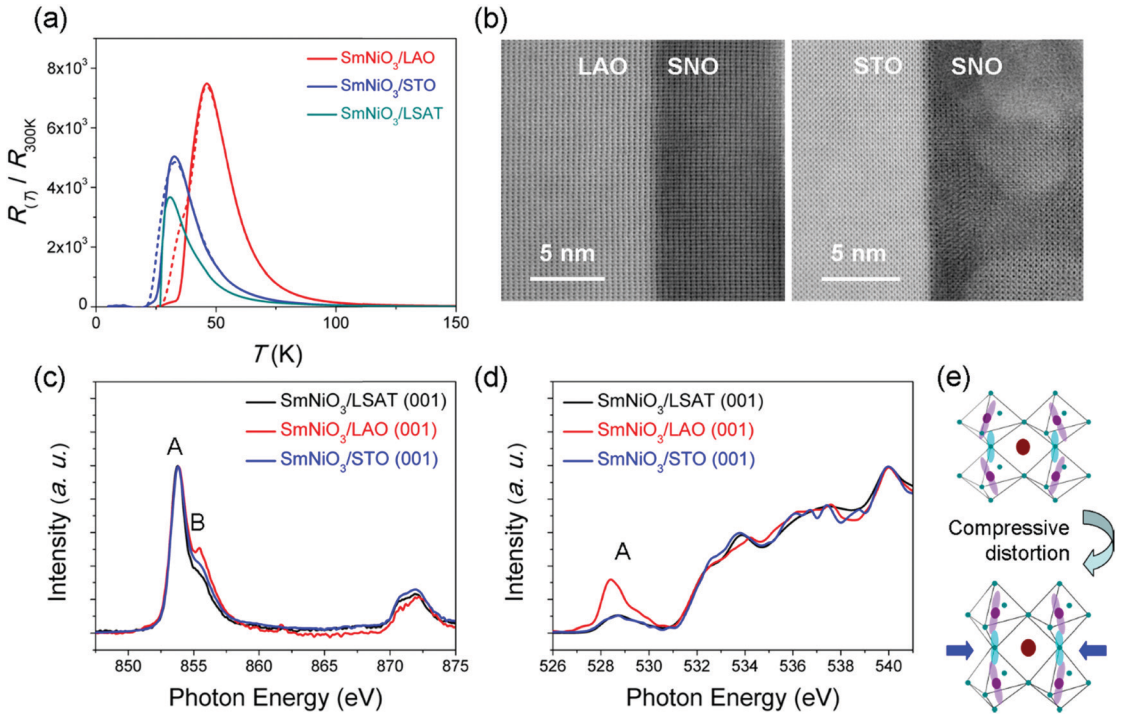

Fig. 2 (a) Temperature-dependence of the material resistivity (R–T) for $SmNiO_3$ (SNO) on the $LaAlO_3$ (LAO), $SrTiO_3$ (STO) and $(LaAlO_3)_{0.3}(Sr_2AlTaO_6)_{0.7}$ (LSAT) substrates with a (001) orientation. The solid lines were measured *via* heating, while the dash lines were measured *via* cooling. (b) Representative cross-section morphologies for $SmNiO_3$/LAO and $SmNiO_3$/STO from high-angle annular dark-field (HAADF). (c–e) Near edge X-ray absorption fine structure (NEXAFS) analysis of the (c) Ni-L_3 edge and (d) O-K edge of $SmNiO_3$ at various states of interfacial strain, while the respective variation in the NiO_6 octahedron under bi-axial compressive distortion is illustrated in (e).

compressive distortion is known to reduce the T_{MIT} of $SmNiO_3$, which is also observed in this work as shown in Fig. S3 (ESI†). To further investigate their electronic structures, near edge X-ray absorption fine structure (NEXAF) analysis was performed to probe the relative variations in the Ni: L-edge and O: K-edge of our samples, as shown in Fig. 2c and d, respectively. Compared to the strain relaxed $SmNiO_3$/$SrTiO_3$ or $SmNiO_3$/(La,Sr)(Al,Ta)O_3, a larger proportion of B within the Ni: L_3 spectrum is observed for the compressively distorted $SmNiO_3$/$LaAlO_3$. This indicates the elevation in the proportion of the $t^6_{2g}e^1_g$ (Ni^{3+}) ground state orbital configuration compared to $t^6_{2g}e^2_g$ (Ni^{2+})[21,22] when imparting the compressive distortion. A consistent variation was further observed in their O: K-edge (Fig. 2d), in which case the pre-peak ($d^8\underline{L}$) for $SmNiO_3$/LAO exhibits a higher intensity.[21,23] In general, the present variation in the relative height of peak B in the Ni-L edge and O-K edge observed in this work is in agreement with the observations made previously in ref. 24.

From the above results, we can see that imparting bi-axial compressive distortion upon $SmNiO_3$ elevates $T_{R\text{-}MIT}$ during the R-MIT, which is not simply associated with the manipulation of the relative electronic phase stability in the MIT as T_{MIT} is reduced. The situation for biaxial tensile distorted $SmNiO_3$, *i.e.* coherently grown on $SrTiO_3$ *via* pulsed laser deposition similar to ref. 24, is demonstrated in Fig. S4 (ESI†), in which case the tensile distortion can be stabilized *via* the kinetics of the plasma involving process.[24,25] The same in-plane lattice vector is observed for the pulsed laser deposited $SmNiO_3$ and the $SrTiO_3$ substrate underneath (see Fig. S4a, ESI), while a coherent interface is observed in between (see Fig. S4b, ESI†). Nevertheless, no R-MIT behavior is observed for the biaxial tensile strained $SmNiO_3$ in the investigated temperature down to 2 K, indicating that $T_{R\text{-}MIT}$ is either eliminated or further reduced below 2K. This observation in the R-MIT is analogous to the MIT of tensile strained $SmNiO_3$, in which case its MIT was not clearly observed.[24,25]

To further regulate $T_{R\text{-}MIT}$ within a broader range of temperature, we adjusted the rare-earth composition occupying the A-sites of the perovskite structures, similar to the regulation of their T_{MIT}.[8,26,27] Reducing the size of the rare-earth element results in a more tilted NiO_6 octahedron, which elevates the metastability in their more distorted perovskite structure, as demonstrated in Fig. 3a. This was previously known to strengthen the insulating phase at high temperature *via* more effectively splitting an energy gap within the hybridized O2p–Ni3d orbits, which elevates T_{MIT}.[8] It is also worth noticing that the enhanced structural distortion when using smaller Re meanwhile reduces the symmetry in the orbital configurations and is expected to reduce the initial S_{Orbit}. This provides a larger thermodynamical potential to trigger the R-MIT at a higher temperature, while the enhanced metastability is expected to kinetically reduce the transition energy barrier.

Our expectation is confirmed by comparing the R–T results measured for $ReNiO_3$ with various single element Re compositions grown on the $LaAlO_3$ substrate, as shown in Fig. 3b. Fig. S5 (ESI†) shows the resistance of the respective samples measured

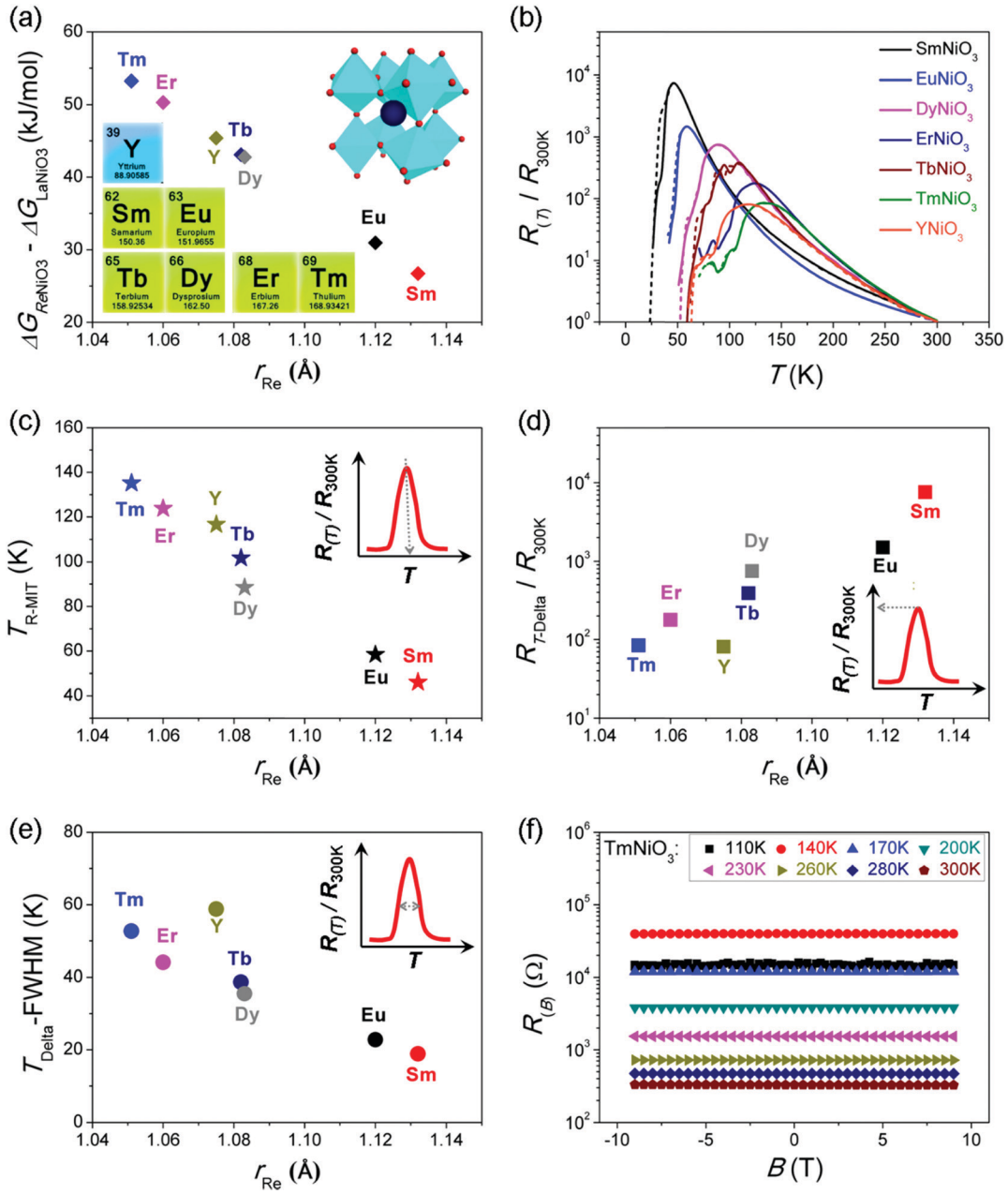

Fig. 3 (a) The elevation in material meta-stability for $ReNiO_3$, compared to the thermodynamically stable $LaNiO_3$, with reducing the size of the rare-earth elements. (b) Temperature-dependence of the material resistivity (R–T) for single rare-earth composition $ReNiO_3$ grown on the $LaAlO_3$ (001) substrate. The solid lines were measured *via* heating, while the dash lines were measured *via* cooling. (c) The reverse metal to insulator transition temperature ($T_{R\text{-}MIT}$), (d) the maximum resistivity at $T_{R\text{-}MIT}$ compared to the one at 300 K, and (e) the full width at half maximum of its resultant delta-shaped temperature dependence with resistivity (T_{Delta}-FWHM) summarized from the R–T of $ReNiO_3$. (f) Resistance of $TmNiO_3$ measured as a function of the imparted external magnetic field (B) at various temperatures.

as a function of temperature. By reducing the size of Re from Sm towards Tm, the temperature to trigger the R-MIT is observed to be elevated from ~50 K to ~150 K, while their $T_{R\text{-}MIT}$ is more clearly compared in Fig. 3c. Meanwhile, the sharpness in the delta-temperatural transport is reduced, as indicated by their smaller variations in resistivity ($R_{T\text{-}Delta}/R_{300K}$) and the broadening of the full width at half maximum of the delta-temperature range (T_{Delta}-FWHM) shown in Fig. 3d and e, respectively. It is also interesting to note that the achieved delta-temperatural transport is relatively stable in a magnetic field up to 10 T, as demonstrated in Fig. 3f for $TmNiO_3/LaAlO_3$ (see more examples in Fig. S6, ESI†). It is worth noticing that the rare-earth composition, as compared to the interfacial strain, should be a more dominant parameter in the regulation of $T_{R\text{-}MIT}$, the situation of which is similar to the regulation of T_{MIT}.[25–27] For example, $SmNiO_3$ exhibits a slightly larger lattice constant compared to $EuNiO_3$, and therefore the $SmNiO_3$ grown on the $LaAlO_3$ substrate is more compressively strained compared to

$EuNiO_3$. Nevertheless, $T_{R\text{-}MIT}$ for $EuNiO_3/LaAlO_3$ is higher than for $SmNiO_3/LaAlO_3$.

Apart from single rare-earth composition $ReNiO_3$, perovskite nickelates with binary and triple rare-earth compositions were also investigated to achieve a more continuous regulation of $T_{R\text{-}MIT}$ and its resultant delta-temperatural transport. It was previously known that for regulating the MIT of rare-earth nickelates, T_{MIT} of $Re_xRe_{1-x}'NiO_3$ is capable of being linearly adjusted between the T_{MIT} of $ReNiO_3$ and $Re'NiO_3$, *via* varying the relative composition of x.[8,26] Fig. 4a shows the R–T relation in the low temperature range for the multiple rare-earth composition perovskite nickelates (see their resistance measured as a function of temperature in Fig. S5, ESI†). In Fig. 4b, we more clearly compare their $T_{R\text{-}MIT}$ with the single rare-earth composition $ReNiO_3$. In contrast to the MIT, it is interesting to note that the observed $T_{R\text{-}MIT:Re,Re'}$ for $Re_xRe_{1-x}'NiO_3$ is always below the calculated one from the composition weighted average of $T_{R\text{-}MIT}$ from $ReNiO_3$ and $Re'NiO_3$, as $[xT_{R\text{-}MIT:Re} + (1-x)T_{R\text{-}MIT:Re'}]$. As can be seen in several representative examples shown in Fig. 4b, $Sm_{3/4}Tm_{1/4}NiO_3$ exhibits a lower $T_{R\text{-}MIT}$ compared to $SmNiO_3$ and $TmNiO_3$; $Sm_{3/4}Eu_{1/4}NiO_3$ exhibits a lower $T_{R\text{-}MIT}$ compared to $SmNiO_3$ and $EuNiO_3$; and $Sm_{3/4}Tm_{1/4}NiO_3$ exhibits a lower $T_{R\text{-}MIT}$ compared to $SmNiO_3$ and $TmNiO_3$.

These results further support our expectation that the R-MIT is entropy related and differs to the MIT in conventional Mott–Hubbard systems as dominantly driven by the orbital Coulomb energy.[8] From the results shown in Fig. 4a and b, we can see that introducing a small proportion of a secondary rare-earth element (*i.e.*, 25%) into the previous one always reduces the $T_{R\text{-}MIT}$, no matter whether the radius of the secondary rare-earth element is larger or smaller than the previous one. This excludes the potential dominance by interfacial strains, since the compressive distortion should be strengthened *via* mixing larger Re and weakened *via* smaller Re. In addition, $U_{Coul.}$ is also not likely to be the dominant reason for such observations, since $U_{Coul.}$ is expected to be monotonically regulated *via* the radius of Re.

Alternatively, it is worth noticing that the difference in rare-earth composition within $ReNiO_3$ is expected to vary the orbital configurations in every degree of freedom within the real space. Therefore, the elevation in $S_{Orbit.}$ on introducing an additional rare-earth composition is expected to be much larger compared to the enhancement in the compositional entropy, which is simply

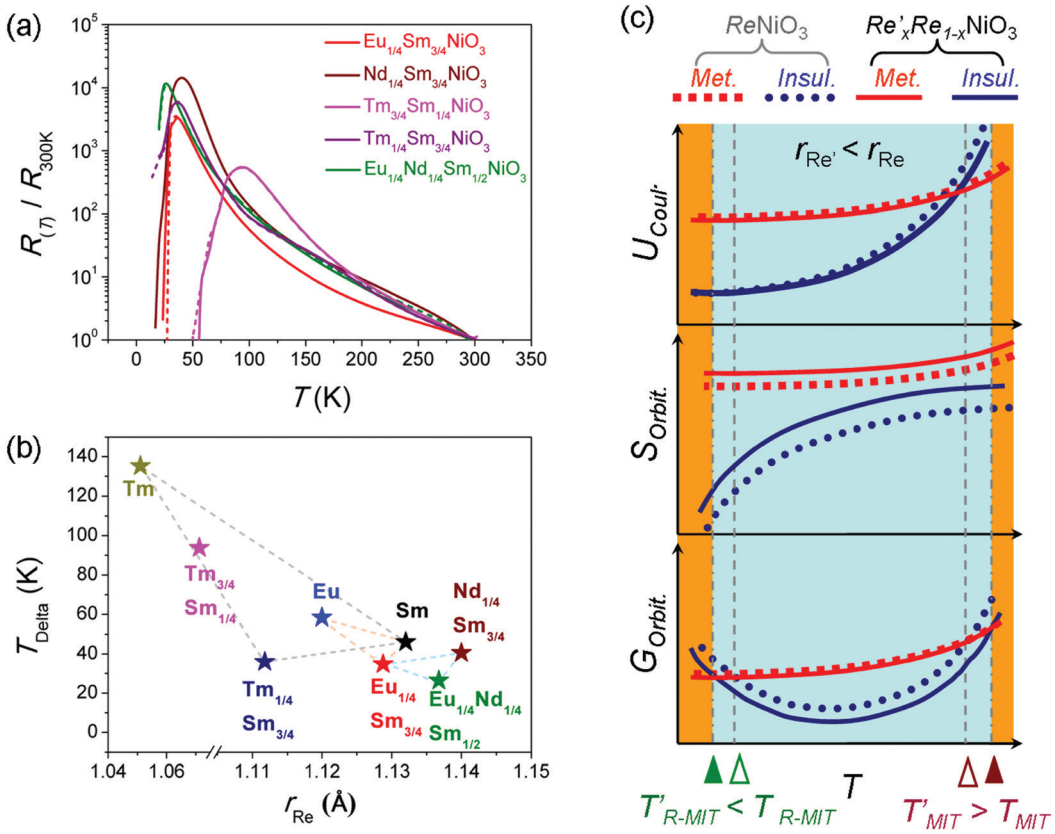

Fig. 4 (a) Temperature-dependence of the material resistivity (R–T) for multiple rare-earth compositional $ReNiO_3$ grown on the $LaAlO_3$ (001) substrate. The solid lines were measured *via* heating, while the dash lines were measured *via* cooling. (b) The reverse metal to insulator transition temperature ($T_{R\text{-}MIT}$) summarized from the R–T of multiple compositional $ReNiO_3$. (c) Illustrating the variations in the Coulomb repulsion energy ($U_{Coul.}$), orbital entropy ($S_{Orbit.}$) and free energy ($G_{Orbit.}$) when substituting the rare-earth composition in $ReNiO_3$ by a smaller rare-earth element (Re′). This is previously known to more distort the NiO_6 octahedron, which opens the band gap and elevates T_{MIT}. Unlike the MIT mainly driven by $U_{Coul.}$, the R-MIT is expected to be triggered by the contribution from the descending $S_{Orbit.}$ to $G_{Orbit.}$ with temperature that offsets the variation in $U_{Coul.}$ between the insulating and metallic phases. The multiple rare-earth composition within $ReNiO_3$ is expected to not only enhance the compositional entropy but also largely enrich the orbital configuration complexity, which elevates $S_{Orbit.}$, and this further results in the reduction in $T_{R\text{-}MIT}$.

calculated as $\Delta S_{EPC} = -k_B\left[x\ \log(x) + (1-x)\log\left(\frac{1-x}{1-N}\right)\right]$.[16] As illustrated in Fig. 4c, the elevation in $S_{Orbit.}$ *via* multiple compositional Re is expected to enhance the negative gain in the entropy contribution to $\Delta G_{Orbit.}$ within the insulating phase of $Re_xRe_{1-x}'NiO_3$, resulting in the reduction of $T_{R\text{-}MIT}$. $R_{T\text{-}Delta}/R_{300K}$ and T_{Delta}-FWHM for multiple rare-earth composition perovskite nickelates are shown in Fig. S5 (ESI†), where a reducing sharpness in delta-temperatural transport is also observed with the elevation of $T_{R\text{-}MIT}$. Although the relationship of $T_{R\text{-}MIT}$ with the multiple-Re compositions is more complex than the one of T_{MIT}, a continuous regulation in the magnitude of $T_{R\text{-}MIT}$ can be still achieved.

It is also worth noticing that the delta-temperatural transportation behavior is not likely to be an intrinsic material property of $ReNiO_3$, as similar transportation behaviors were not observed for their polycrystalline bulk counterparts. Instead, more complex extrinsic factors such as defects and interfaces could be also the cause of the observed R-MIT. Nevertheless, the achieved delta-temperatural transport is expected to open up a new door for exploring new applications, such as more conveniently locking/excluding the working conditions of electric devices and circuits within a narrow window of temperature.

4. Conclusions

To sum up, a reverse temperature-dependence in the electrical transportation tendency as compared to the MIT (denoted as the R-MIT) was observed at a low temperature range within chemically grown $ReNiO_3$ with large meta-stability (*i.e.*, size of Re < Nd) on single crystalline perovskite substrates. We achieved broad regulation in its transition point ($T_{R\text{-}MIT}$) *via* adjusting the rare-earth composition or imparting interfacial strains. The R-MIT is expected to be entropy related, and its transition temperature is possible to elevate *via* imparting compressive interfacial strains, or reducing the size and compositional complexity of the rare-earth elements. From the aspect of application, a distinguished character of delta-temperatural transport is achieved *via* combining the R-MIT and afterwards NTCR thermistor transportation of $ReNiO_3$ by elevating the temperature across $T_{R\text{-}MIT}$. It results in a significant enhancement in the electronic resistivity within a narrow window of temperature, and is expected to result in new applications such as locking the working temperature range for electric devices catering for the demand in fast developing automatic transmission or artificial intelligence.

Author contributions

JC proposed the original idea, planned the work, partially performed the experiments (*i.e.*, sample growth, structure and transport characterization), analysed the data, and wrote the manuscript; HH contributed to the sample growth and transport characterization; HD and BG contributed to the TEM experiment; JW contributed to the EXAFS experiment; TY provided constructive discussions; NC and YJ provided constructive support in the aspects of sample growth and characterization, respectively.

Conflicts of interest

We declare no competing financial interest.

Acknowledgements

This work was supported by the National Natural Science Foundation of China (No. 51602022 and 61674013). We also acknowledge the constructive discussions with Prof. Rafael Jaramillo from MIT, USA and Prof. Shriram Ramanathan from Purdue University, USA, as well as the technical support from Prof. Akira Toriumi from the University of Tokyo and Prof. Lidong Chen from Shanghai Institute of Ceramics Chinese Academy of Sciences.

References

1 N. Lu, P. Zhang, Q. Zhang, R. Qiao, Q. He, H. B. Li, Y. Wang, J. Guo, D. Zhang, Z. Duan, Z. Li, M. Wang, S. Yang, M. Yan, E. Arenholz, S. Zhou, W. Yang, L. Gu, C. W. Nan, J. Wu, Y. Tokura and P. Yu, Electric-field control of tri-state phase transformation with a selective dual-ion switch, *Nature*, 2017, **546**, 124.

2 H. H. Kung, R. E. Baumbach, E. D. Bauer, V. K. Thorsmølle, W. L. Zhang, K. Haule, J. A. Mydosh and G. Blumberg, Chirality density wave of the ''hidden order'' phase in URu_2Si_2, *Science*, 2015, **347**, 1339–1342.

3 L. J. Li, E. C. T. O'Farrell, K. P. Loh, G. Eda, B. Özyilmaz and A. H. C. Neto, Controlling many-body states by the electric-field effect in a two-dimensional material, *Nature*, 2016, **529**, 185.

4 Z. Zhang, D. Schwanz, B. Narayanan, M. Kotiuga, J. A. Dura, M. Cherukara, H. Zhou, J. W. Freeland, J. Li, R. Sutarto, F. He, C. Wu, J. Zhu, Y. Sun, K. Ramadoss, S. S. Nonnenmann, N. Yu, R. Comin, K. M. Rabe, S. K. R. S. Sankaranarayanan and S. Ramanathan, Rerovskite nickelates as electric-field sensor in salt water, *Nature*, 2018, **553**, 68.

5 Y. Zhou, X. Guan, H. Zhou, K. Ramadoss, S. Adam, H. Liu, S. Lee, J. Shi, M. Tsuchiya, D. D. Fong and S. Ramanathan, Strongly correlated perovskite fuel cells, *Nature*, 2016, **534**, 231.

6 J. Shi, Y. Zhou and S. Ramanathan, Colossal resistance switching and band gap modulation in a perovskite nickelate by electron doping, *Nat. Commun.*, 2014, **5**, 4860.

7 J. B. Goodenough, The two components of crystallographic transition in VO_2, *J. Solid State Chem.*, 1971, **3**, 490–500.

8 G. Catalan, Progress in perovskite nickelate research, *Phase Transitions*, 2008, **81**, 729.

9 K. Shibuya, M. Kawasaki and Y. Tokura, Metal-insulator transition in epitaxial $V_{1-}xWxO_2$ ($0 < x < 0.33$) thin films, *Appl. Phys. Lett.*, 2010, **96**, 022102.

10 F. Guo, S. Chen, Z. Chen, H. Luo, Y. Gao, T. Przybilla, E. Spiecker, A. Osvet, K. Forberich and C. J. Brabec, Printed

smart photovoltaic window integrated with an energy-saving thermochromic layer, *Adv. Opt. Mater.*, 2015, **3**, 1524–1529.

11 J. Chen, H. Hu, J. Wang, T. Yajima, B. Ge, X. Ke, H. Dong, Y. Jiang and N. Chen, Overcoming synthetic metastabilities and revealing metal-to-insulator transition & thermistor bi-functionalities for d-band correlation perovskite nickelates, *Mater. Horizons*, 2019, **6**, 788.

12 J. Shi, S. D. Ha, Y. Zhou, F. Schoofs and S. Ramanathan, A correlated nickelate synaptic transistor, *Nat. Commun.*, 2013, **4**, 2676.

13 K. Martens, J. W. Jeong, N. Aetukuri, C. Rettner, N. Shukla, E. Freeman, D. N. Esfahani, F. M. Peeters, T. Topuria, P. M. Rice, A. Volodin, B. Douhard, W. Vandervorst, M. G. Samant, S. Datta and S. S. P. Parkin, Field effect and strongly localized carriers in the metal-insulator transition material VO_2, *Phys. Rev. Lett.*, 2015, **115**, 196401.

14 T. Yajima, T. Nishimura and A. Toriumi, Positive-bias gate-controlled metal–insulator transition in ultrathin VO_2 channels with TiO_2 gate dielectrics, *Nat. Commun.*, 2015, **6**, 10104.

15 F. Zuo, P. Panda, M. Kotiuga, J. Li, M. Kang, C. Mazzoli, H. Zhou, A. Barbour, S. Wilkins, B. Narayanan, M. Cherukara, Z. Zhang, S. K. R. S. Sankaranarayanan, R. Comin, K. M. Rabe, K. Roy and S. Ramanathan, Habituation based synaptic plasticity and organismic learning in a quantum perovskite, *Nat. Commun.*, 2017, **8**, 240.

16 J. D. Budai, J. Hong, M. E. Manley, E. D. Specht, C. W. Li, J. Z. Tischler, D. L. Abernathy, A. H. Said, B. M. Leu, L. A. Boatner, R. J. McQueeney and O. Delaire, Metallization of vanadium dioxide driven by large phonon entropy, *Nature*, 2014, **515**, 535.

17 C. M. Rost, E. Sachet, T. Borman, A. Moballegh, E. C. Dickey, D. Hou, J. L. Jones, S. Curtarolo and J. P. Maria, Entropy-stabilized oxides, *Nat. Commun.*, 2015, **6**, 8485.

18 I. I. Mazin, D. I. Khomskii, R. Lengsdorf, J. A. Alonso, W. G. Marshall, R. M. Ibberson, A. Podlesnyak, M. J. Martínez-Lope and M. M. Abd-Elmeguid, Charge Ordering as Alternative to Jahn-Teller Distortion, *Phys. Rev. Lett.*, 2007, **98**, 176406.

19 J. S. Zhou and J. B. Goodenough, Chemical bonding and electronic structure of RNiO$_3$ (R = rare earth), *Phys. Rev. B: Condens. Matter Mater. Phys.*, 2004, **69**, 153105.

20 J. A. Alonso, J. L. García-Muñoz, M. T. Fernández-Díaz, M. A. G. Aranda, M. J. Martínez-Lope and M. T. Casais, Charge Disproportionation in RNiO$_3$ Perovskites: Simultaneous metal-insulator and structural transition in YNiO$_3$, *Phys. Rev. Lett.*, 1999, **82**, 3871.

21 K. Kleiner, J. Melke, M. Merz, P. Jakes, P. Nage, S. Schuppler, V. Liebau and H. Ehrenberg, Unraveling the degradation process of $LiNi_{0.8}Co_{0.15}Al_{0.05}O_2$ electrodes in commercial lithium ion batteries by electronic structure investigations, *ACS Appl. Mater. Interfaces*, 2015, **7**, 19589.

22 L. A. Montoro, M. Abbate and J. M. Rosolen, Electronic structure of transition metal Ions in deintercalated and reintercalated $LiCo_{0.5}Ni_{0.5}O_2$, *J. Electrochem. Soc.*, 2000, **147**, 1651–1657.

23 F. Reinert, P. Steiner, S. Hüfner, H. Schmitt, J. Fink, M. Knupfer, P. Sandl and E. Bertel, Electron and hole doping in NiO, *Z. Phys. B: Condens. Matter*, 1995, **97**, 83–93.

24 J. Chen, W. Mao, B. Ge, J. Wang, X. Ke, V. Wang, Y. Wang, M. Döbeli, W. Geng, H. Matsuzaki, J. Shi and Y. Jiang, Revealing the role of lattice distortions in the hydrogen-induced metal-insulator transition of $SmNiO_3$, *Nat. Commun.*, 2019, **10**, 694.

25 F. Conchon, A. Boulle and R. Guinebretière, Effect of tensile and compressive strains on the transport properties of $SmNiO_3$ layers epitaxially grown on (001) $SrTiO_3$ and $LaAlO_3$ substrates, *Appl. Phys. Lett.*, 2007, **91**, 192110.

26 A. Ambrosini and J. F. Hamet, SmxNd$_{1-x}$NiO$_3$ thin-film solid solutions with tunable metal–insulator transition synthesized by alternate-target pulsed-laser deposition, *Appl. Phys. Lett.*, 2003, **82**, 727.

27 M. T. Escote, A. M. L. da Silva, J. R. Matos and R. F. Jardim, General properties of polycrystalline LnNiO$_3$ (Ln = Pr, Nd, Sm) compounds prepared through different precursors, *J. Solid State Chem.*, 2000, **151**, 298–307.

